

Cite this: *Chem. Sci.*, 2024, 15, 18634

All publication charges for this article have been paid for by the Royal Society of Chemistry

Construction of covalent organic frameworks *via* the Mannich reaction at room temperature for light-driven oxidative hydroxylation of arylboronic acids†

Jian-Cheng Wang,^{‡*} Ting Sun,[‡] Jun Zhang, Zhi Chen, Jia-Qi Du, Jing-Lan Kan and Yu-Bin Dong^{‡*}Received 2nd July 2024
Accepted 16th October 2024

DOI: 10.1039/d4sc04358h

rsc.li/chemical-science

An increasing variety of organic reactions have been developed for the synthesis of more structurally stable and multifunctional COFs. Here, we report a class of β -ketamine linked covalent organic frameworks that were constructed through the CeCl_3 -catalyzed multi-component Mannich reaction at room temperature. And the TAD-COF obtained based on this method could significantly promote the light-driven oxidative hydroxylation of arylboronic acids.

Introduction

Covalent organic frameworks (COFs) are functional crystalline porous supramolecular materials formed through the covalent bonding of specific organic monomers *via* organic reactions. Since their first synthesis by the Yaghi team in 2005,¹ COFs have found extensive applications across various fields due to their well-defined structure, pre-designability, high porosity, excellent thermal stability, strong chemical stability, and ease of functionalization.² Over the past 20 years, research on COFs has primarily focused on two aspects: developing novel synthesis methods and exploring new properties and applications.³

The composition, function, and stability of COFs largely rely on the choice of organic monomers as well as the covalent bonds formed between them. Currently, most COFs are constructed using reversible boron ester or imine bonding.⁴ While this reversibility allows for self-regulation and facilitated crystallization of COF crystals, it also poses limitations on their chemical stability for further application development. To address these challenges related to chemical stability issues, scientists have conducted extensive research work by altering the types of covalent bonds used to synthesize chemically stable COFs.⁵ In addition to classic reactions such as the boric acid self-coupling reaction and Schiff base reaction that are commonly employed in synthesizing COFs, an increasing

number of other organic synthesis reactions such as the Knoevenagel condensation reaction,⁶ Debus–Radziszewski reaction,⁷ Strecker reaction,⁸ Povarov reaction,⁹ A^3 coupling reaction,¹⁰ Groebke–Blackburn–Bienaymé reaction,¹¹ Doebner reaction,¹² Kabachnik–Fields reaction,¹³ and Petasis reaction¹⁴ are being utilized at present. The Mannich reaction,¹⁵ being a highly significant organic transformation, affords an important nitrogen-containing heterocyclic compound known as the Mannich base, which possesses remarkable structural stability. However, to date, with the exception of the recent report by the Cui group on synthesis of COFs *via* the Mannich reaction under high-temperature solvent thermal conditions,¹⁵ there are currently no documented instances of synthesis of COFs *via* the Mannich reaction at room temperature. Given the inherent pre-designability of COF structures, we firmly believe that judicious selection of suitable organic monomers can enable the construction of COFs through the employment of the Mannich reaction.

Furthermore, owing to the distinctive advantages of the COF structure, such as well-ordered arrangement, an extensive conjugated system, facile modification of functional groups, excellent photostability, and high light absorption capacity, they have found widespread applications in the field of photocatalysis.¹⁶

In this study, we present for the first time the successful synthesis of β -ketamine-linked COFs using the Mannich reaction at room temperature. Under ambient conditions and in the presence of CeCl_3 as a catalyst, we effectively fabricated a novel class of β -ketamine-linked COFs through the Mannich condensation reaction involving aromatic aldehydes, aromatic amines, and acetophenones. Moreover, one of the obtained COFs, namely TAD-COF, demonstrated exceptional optical activity and served as an efficient heterogeneous photocatalyst

College of Chemistry, Chemical Engineering and Materials Science, Collaborative, Innovation Center of Functionalized Probes for Chemical Imaging in Universities of Shandong, Key Laboratory of Molecular and Nano Probes, Ministry of Education, Shandong Normal University, Jinan 250014, P. R. China. E-mail: wangjiancheng1003@163.com; yubindong@sdsu.edu.cn

† Electronic supplementary information (ESI) available. See DOI: <https://doi.org/10.1039/d4sc04358h>

‡ These authors contributed equally.

for the visible-light-driven oxidation hydroxylation of arylboronic acids.

Results and discussion

As shown in Scheme 1, the model reaction among benzaldehyde, acetophenone, and aniline afforded model compound 1,3-diphenyl-3-(phenylamino)propan-1-one in 86% yield in the presence of CeCl_3 and anhydrous methanol at room temperature (ESI†). Based on this, we performed the Mannich condensation reaction synthesis of COFs from the corresponding monomers. As a result, the β -ketoamine-linked **TAD-COF** was successfully synthesized *via* Mannich condensation polymerization of 4,4',4''-(1,3,5-triazine-2,4,6-triyl)tribenzaldehyde (TATB), acetophenone (AP), and 4,4'-diaminodiphenyl (DADP) in 75.1% yield as dark red crystalline solids with the assistance of CeCl_3 (Scheme 1). After screening, the optimized conditions were established as crystallization at room temperature for 7 days in anhydrous methanol and CH_3CN . Despite the longer synthesis time required, this method is relatively environmentally friendly and gentle compared to other high-temperature and high-pressure conditions. The as-synthesized **TAD-COF** was characterized by Fourier transform infrared spectroscopy (FT-IR) and solid-state CP-MAS spectroscopy. Subsequently, the formation of **TAD-COF** was confirmed and the introduction of the β -ketoamine structure was clearly demonstrated (ESI†).

As shown in Fig. 1a, the assessed powder X-ray diffraction (PXRD) pattern indicated that **TAD-COF** had good crystalline

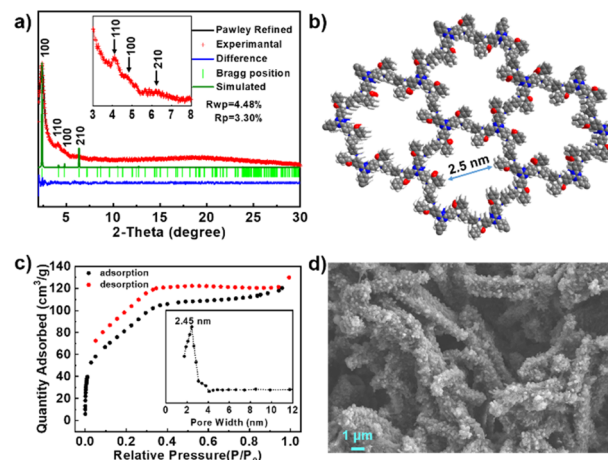
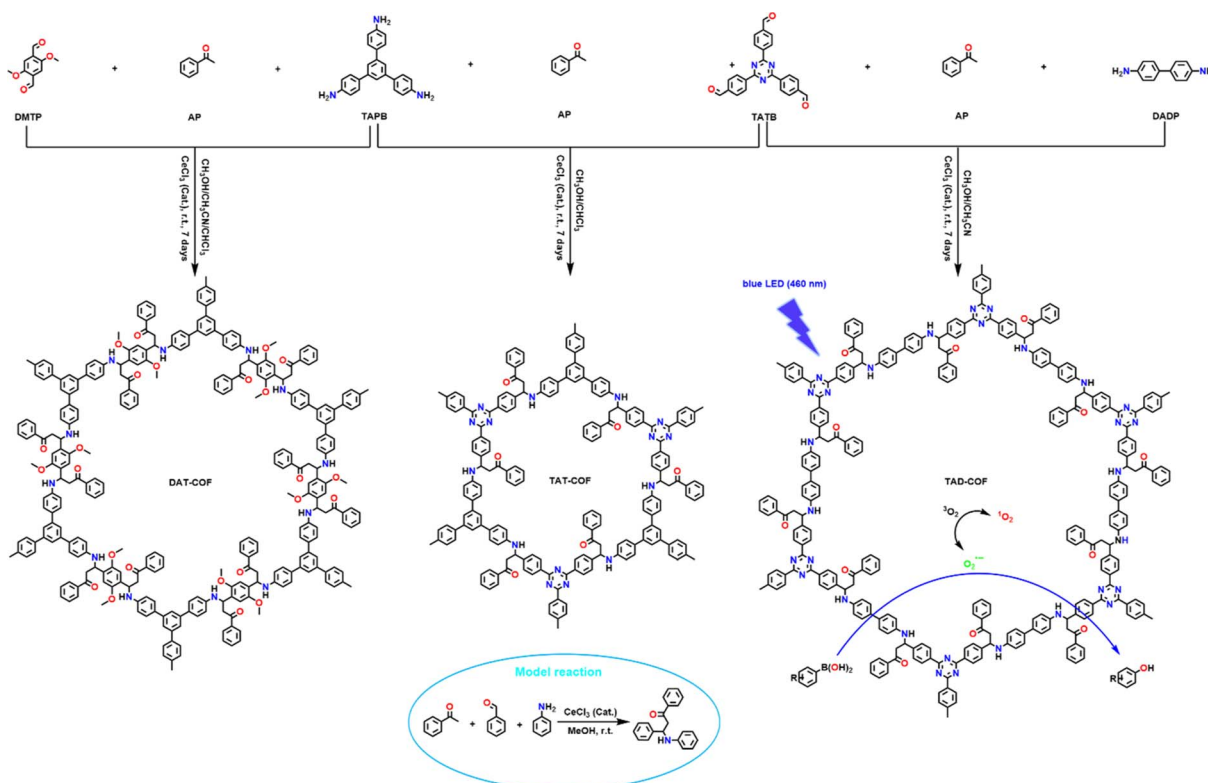


Fig. 1 (a) PXRD patterns of **TAD-COF** (AA stacking). (b) The top view of **TAD-COF** (AA stacking). (c) N_2 adsorption and desorption isotherm of **TAD-COF** measured at 77 K. (Inset: the pore size distribution of **TAD-COF** derived from NLDFT). (d) SEM image of **TAD-COF**.

properties and featured a main peak at 2.375° , which corresponded to the (100) plane, along with three weak peaks at 4.166° , 4.774° , and 6.366° , and these weak peaks were associated with the (110), (100), and (210) planes, respectively. Using Materials Studio software (ver. 2018) to model its structure (ESI†),¹⁷ the most reasonable structure of **TAD-COF** was determined as a 2D layered hexagonal network with eclipsed (AA) stacking mode (Fig. 1b). In addition, **TAD-COF** was crystallized



Scheme 1 Synthesis of **DAT-COF**, **TAT-COF** and **TAD-COF** *via* the CeCl_3 -catalyzed Mannich reaction, with the corresponding model reaction in the inset and the application of **TAD-COF** for light-driven oxidative hydroxylation of arylboronic acids.



in the *P6* space group with unit cell parameters of $a = b = 42.5183 \text{ \AA}$, $c = 3.7231 \text{ \AA}$, $\alpha = \beta = 90^\circ$, and $\gamma = 120^\circ$ (ESI†). To demonstrate the porosity of COF, nitrogen adsorption and desorption experiments were carried out at 77 K. As shown in Fig. 1c, the nitrogen adsorption amount of **TAD-COF** was $130 \text{ cm}^3 \text{ g}^{-1}$, and its corresponding surface area was $315 \text{ m}^2 \text{ g}^{-1}$, based on the Brunauer–Emmett–Teller (BET) model calculation. Notably, hysteresis was observed across the multilayer range of the physical adsorption isotherm, which was typically associated with capillary condensation in mesoporous structures.¹⁸ The pore size distribution curve based on nonlocal density functional theory (NLDFT) analysis demonstrated that **TAD-COF** had a pore size distribution center at about 2.45 nm (Fig. 1c), which was consistent with the theoretical simulation structure (Fig. 1b). The SEM image showed that the **TAD-COF** possessed homogeneous wire-shaped morphology composed of micro-nano particles (Fig. 1d and ESI†).

Thermogravimetric analysis (TGA) indicated that **TAD-COF** experienced almost no weight loss before 400 °C, indicating its good thermal stability (Fig. 2a). In addition, **TAD-COF** is stable enough against some organic (DMF and EtOH), basic (NaOH aqueous solution, 6 M) and acidic (HCl aqueous solution, 2 M) media (ESI†). As shown in the solid state ultraviolet-visible (UV-vis) spectrum, the obtained **TAD-COF** has three absorption bands in the range of 200–500 nm (centered at ~272 nm, 365 nm and 460 nm, respectively) (Fig. 2b), and the corresponding optical band gap (E_g) of **TAD-COF** was calculated to be 1.42 eV by a Tauc plot (Fig. 2c).¹⁹ Additionally, a visible blue (460 nm for **TAD-COF**) LED was selected as the excitation light source to test their photodynamic properties. As shown in Fig. 2d, **TAD-COF** showed a fast photocurrent response and repeated intermittent switch irradiation cycles, which provided direct evidence for photo-induced carrier transfer in the COFs. The above results clearly demonstrate that **TAD-COF** has the potential to serve as a promising photocatalyst.

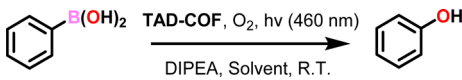
To better illustrate the photocatalytic activity of **TAD-COF** in organic conversion, we selected the photo-induced oxidation

hydroxylation reaction of arylboronic acid as the organic reaction. The oxidation hydroxylation reaction of arylboronic acid for the synthesis of phenol from arylboronic acid is a commonly encountered organic transformation, yielding phenolic compounds that are widely utilized as important chemical raw materials in various industries, agriculture, medicine, and fine chemicals.²⁰ Initially, the oxidation hydroxylation reaction of phenylboronic acid catalyzed by **TAD-COF** was selected as the model reaction to optimize the reaction conditions (Table 1).

To achieve the optimal reaction conditions, various factors affecting the reaction effect, such as solvent type, reaction time, sacrificial agent dosage, and different amounts of catalyst, were comprehensively investigated *via* the control experiments (Table 1, entries 1–11). In an oxygen atmosphere, when **TAD-COF** was used as a catalyst and the amount of **TAD-COF** was 10 mg, the amount of DIPEA was 5 eq., and the reaction time was 9 h in $\text{CH}_3\text{CN}/\text{H}_2\text{O}$ (4/1, v/v), providing the best results, and the final yield of phenol was 99% (Table 1, entry 6). To verify that **TAD-COF** played an indispensable role, corresponding experiments were also carried out. With no catalyst, none of the product was obtained (Table 1, entry 12). When air replaces oxygen, the yield of the reaction was only 28% (Table 1, entry 13). Also, the reaction cannot proceed smoothly in the absence of light or oxygen (Table 1, entries 14 and 15).

The leaching test fully verified the heterogeneous catalysis properties of **TAD-COF**, and no further reaction occurred without **TAD-COF** after treating the oxidation hydroxylation reaction of phenylboronic acid after 3 h (ESI†). In addition, **TAD-COF** could be easily recovered through centrifugation and directly reused for the next catalytic run under the same

Table 1 Optimization of reaction conditions for the model oxidation hydroxylation reaction of phenylboronic acid^a

|  | | | | | |
|--|------------------------|---|--------------|--------------|------------------------|
| Entry | TAD-COF (mg) | Solvent (2 mL) | DIPEA | <i>t</i> (h) | Yield ^b (%) |
| 1 | 10 | CH_3CN | 5 eq. | 12 | 87 |
| 2 | 10 | DMF | 5 eq. | 12 | 81 |
| 3 | 10 | H_2O | 5 eq. | 12 | 86 |
| 4 | 10 | $\text{CH}_3\text{CN} : \text{H}_2\text{O}$ (4 : 1) | 5 eq. | 12 | 99 |
| 5 | 10 | $\text{CH}_3\text{CN} : \text{H}_2\text{O}$ (1 : 1) | 5 eq. | 12 | 85 |
| 6 | 10 | $\text{CH}_3\text{CN} : \text{H}_2\text{O}$ (4:1) | 5 eq. | 9 | 99 |
| 7 | 10 | $\text{CH}_3\text{CN} : \text{H}_2\text{O}$ (4 : 1) | 5 eq. | 6 | 95 |
| 8 | 10 | $\text{CH}_3\text{CN} : \text{H}_2\text{O}$ (4 : 1) | 3 eq. | 9 | 80 |
| 9 | 10 | $\text{CH}_3\text{CN} : \text{H}_2\text{O}$ (4 : 1) | 7 eq. | 9 | 99 |
| 10 | 7 | $\text{CH}_3\text{CN} : \text{H}_2\text{O}$ (4 : 1) | 5 eq. | 9 | 83 |
| 11 | 15 | $\text{CH}_3\text{CN} : \text{H}_2\text{O}$ (4 : 1) | 5 eq. | 9 | 99 |
| 12 | 0 | $\text{CH}_3\text{CN} : \text{H}_2\text{O}$ (4 : 1) | 5 eq. | 9 | N.D. |
| 13 ^c | 10 | $\text{CH}_3\text{CN} : \text{H}_2\text{O}$ (4 : 1) | 5 eq. | 9 | 29 |
| 14 ^d | 10 | $\text{CH}_3\text{CN} : \text{H}_2\text{O}$ (4 : 1) | 5 eq. | 9 | N.D. |
| 15 ^e | 10 | $\text{CH}_3\text{CN} : \text{H}_2\text{O}$ (4 : 1) | 5 eq. | 9 | N.D. |

^a Reaction conditions: phenylboronic acid (0.5 mmol), **TAD-COF** (7–15 mg), DIPEA (*N,N*-diisopropylethylamine), solvent (2.5 mL) in O_2 .

^b Isolated yields. The products were determined using NMR and MS spectra (ESI). ^c In air. ^d Without light. ^e In N_2 . N. D.: not detected.

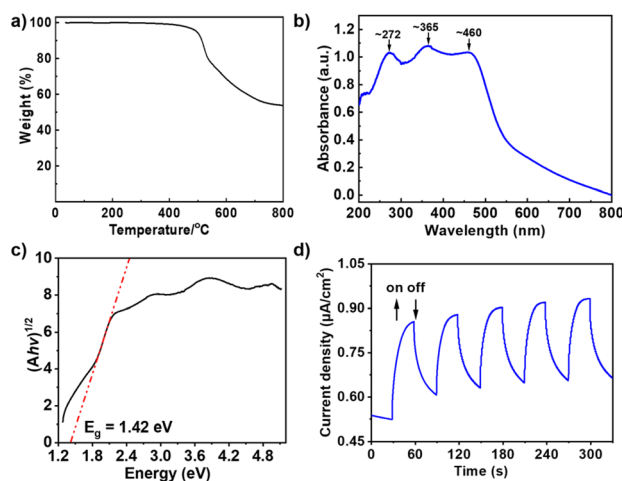


Fig. 2 (a) TGA of **TAD-COF**. (b) UV-vis absorption spectrum of **TAD-COF**. (c) The bandgap of **TAD-COF**. (d) Transient photocurrent of **TAD-COF**.



conditions. As shown in Fig. 3a, the yield still reached 95% at the sixth cycle. After multiple catalytic runs, the structural integrity, high porosity and excellent thermal stability of **TAD-COF** were well maintained, as demonstrated by its PXRD patterns (Fig. 3b), N_2 adsorption and desorption isotherm and pore size distribution (Fig. 3c), and TGA curve (Fig. 3d). More importantly, compared to some previously reported catalysts, **TAD-COF** exhibited excellent catalytic properties (ESI†).

We also investigated the scope of oxidative hydroxylation of arylboronic acids catalyzed by **TAD-COF** using different substituted arylboronic acids as substrates (Table 2, **2a–2o**). With the exception of a few substrates, such as **2b** (83%), **2k** (88%) and **2l** (89%), all other substrates demonstrated favorable yields, with the yields all exceeding 90%. So, we believed that the catalytic activity of **TAD-COF** was almost not affected by the electronic effect and space effect of substituents in oxidative hydroxylation of arylboronic acids.

Furthermore, we investigated the mechanism of the **TAD-COF**-catalyzed oxidative hydroxylation of arylboronic acids. Initially, we confirmed the presence of reactive oxygen species (ROS) generated during the reaction process through an electron paramagnetic resonance (EPR) spin trapping experiment, with the results indicating the existence of $O_2^{\cdot-}$ and 1O_2 (ESI†). Subsequently, a series of control experiments were conducted by separately introducing capture agents 5,5-dimethyl-1-pyrroline *N*-oxide (DMPO) for $O_2^{\cdot-}$ and 2,2,6,6-tetramethylpiperidine (TEMP) for 1O_2 ,¹⁴ revealing a significant decrease in yield upon addition of DMPO (ESI†). Based on the above experimental findings and relevant literature,²¹ we proposed a potential mechanism: upon exposure to blue LED light, an excited **TAD-COF** was produced, leading to the formation of superoxide radicals *via* single electron transfer (SET) from the excited **TAD-COF** to oxygen, followed by a sequence of free radical quenching, rearrangement, and hydrolysis processes ultimately resulting in phenol product formation (Fig. 4).

Table 2 Substrate scope of the **TAD-COF**-catalyzed oxidative hydroxylation of arylboronic acids^{a,b}

| | | | | |
|---------|---------|---------|---------|---------|
| | | | | |
| | | | | |
| 2a: 99% | 2b: 83% | 2c: 91% | 2d: 97% | 2e: 96% |
| | | | | |
| 2f: 96% | 2g: 97% | 2h: 96% | 2i: 90% | 2j: 94% |
| | | | | |
| 2k: 88% | 2l: 89% | 2m: 95% | 2n: 92% | 2o: 96% |

^a Reaction conditions: arylboronic acids (0.5 mmol), DIPEA (2.5 mmol, 5 eq.), **TAD-COF** (10 mg), CH_3CN/H_2O (4/1, v/v) (2.5 mL), blue LED (460 nm) irradiation for 9 h in an O_2 atmosphere at 25 °C. ^b Isolated yields. The products were determined using NMR and MS spectra (ESI).

Moreover, to confirm the universality of the multi-component Mannich reaction catalyzed by cerium chloride in COF synthesis, two additional COFs (denoted as **DAT-COF** and **TAT-COF**) were successfully synthesized using different monomers *via* the $CeCl_3$ -catalyzed multi-component Mannich reaction under ambient conditions (Scheme 1, ESI†).

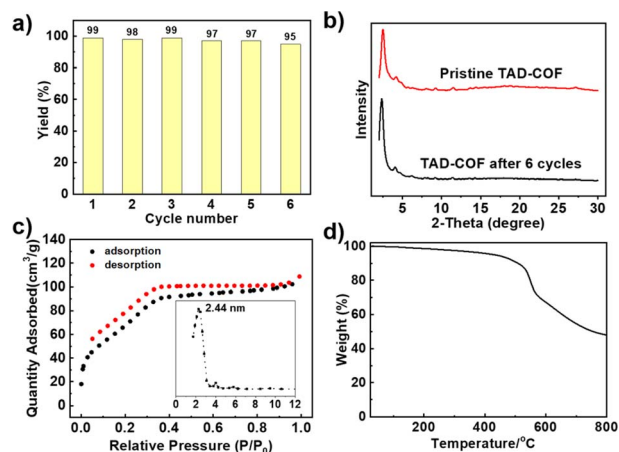


Fig. 3 (a) Catalytic cycle. (b) PXRD patterns of **TAD-COF** and **TAD-COF** after catalytic runs. (c) N_2 adsorption and desorption isotherm of **TAD-COF** after catalytic runs measured at 77 K. (Inset: the pore size distribution of **TAD-COF** after catalytic runs derived from NLDFT). (d) TGA of **TAD-COF** after catalytic runs.

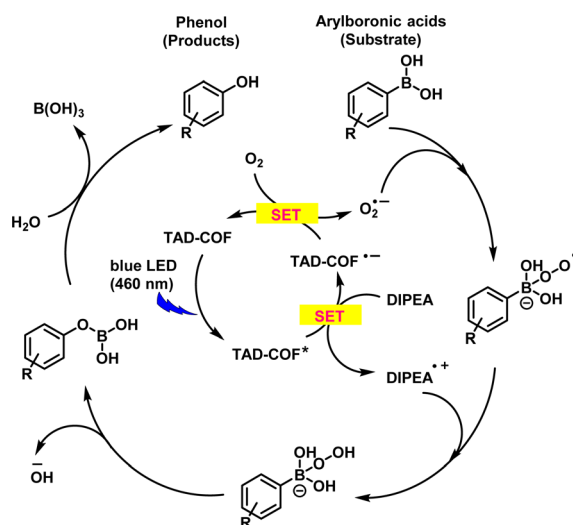


Fig. 4 Proposed possible mechanism for the photocatalytic transformation of arylboronic acids into corresponding phenols in the presence of **TAD-COF**. SET: Single Electron Transfer.



Conclusions

In conclusion, we reported a novel approach for synthesizing COFs through the Mannich reaction at room temperature, resulting in the successful synthesis of a series of COFs. Furthermore, the TAD-COF obtained by this method acted as a catalyst for achieving the photocatalytic transformation of arylboronic acids into corresponding phenols. We believe that employing the multi-component Mannich reaction for the synthesis of COFs can not only effectively broaden the array of methods for constructing COF materials through organic reactions, but also yield structurally robust and functionally potent COFs.

Data availability

The data that support the findings of this study are presented in the paper and the ESI.†

Author contributions

All authors contributed extensively to the work presented in this paper. Y.-B. Dong and J.-C. Wang conceived the research project. T. Sun performed the experiments and the data analyses. J. Zhang, Z. Chen, J.-Q. Du and J.-L. Kan assisted with the data collection. J.-C. Wang and Y.-B. Dong wrote the manuscript with the input from the other authors.

Conflicts of interest

There are no conflicts to declare.

Acknowledgements

We are grateful for financial support from NSFC (Grants 22371172 and 21971153), the Major Basic Research Projects of the Shandong Natural Science Foundation (No. ZR2020ZD32), the Youth Innovation Science and Technology Program of Higher Education Institution of Shandong Province (No. 2022KJ253), and the Taishan Scholars Climbing Program of Shandong Province.

References

- 1 P. Côté Adrien, I. Benin Annabelle, W. Ockwig Nathan, M. O'Keeffe, J. Matzger Adam and M. Yaghi Omar, *Science*, 2005, **310**, 1166–1170.
- 2 (a) K. Geng, T. He, R. Liu, S. Dalapati, K. T. Tan, Z. Li, S. Tao, Y. Gong, Q. Jiang and D. Jiang, *Chem. Rev.*, 2020, **120**, 8814–8933; (b) X. Guan, F. Chen, Q. Fang and S. Qiu, *Chem. Soc. Rev.*, 2020, **49**, 1357–1384; (c) C. S. Diercks and O. M. Yaghi, *Science*, 2017, **355**, eaal1585; (d) Y. Liu, X. Liu, A. Su, C. Gong, S. Chen, L. Xia, C. Zhang, X. Tao, Y. Li, Y. Li, T. Sun, M. Bu, W. Shao, J. Zhao, X. Li, Y. Peng, P. Guo, Y. Han and Y. Zhu, *Chem. Soc. Rev.*, 2024, **53**, 502–544.
- 3 (a) S.-Y. Ding and W. Wang, *Chem. Soc. Rev.*, 2013, **42**, 548–568; (b) Q. Guan, L.-L. Zhou and Y.-B. Dong, *J. Am. Chem. Soc.*, 2023, **145**, 1475–1496; (c) Q. Guan, L.-L. Zhou and Y.-B. Dong, *Chem. Soc. Rev.*, 2022, **51**, 6307–6416; (d) J. L. Segura, S. Royuela and M. Mar Ramos, *Chem. Soc. Rev.*, 2019, **48**, 3903–3945; (e) H. Wang, H. Wang, Z. Wang, L. Tang, G. Zeng, P. Xu, M. Chen, T. Xiong, C. Zhou, X. Li, D. Huang, Y. Zhu, Z. Wang and J. Tang, *Chem. Soc. Rev.*, 2020, **49**, 4135–4165; (f) Y. Zhi, Z. Wang, H.-L. Zhang and Q. Zhang, *Small*, 2020, **16**, 2001070.
- 4 R. Liu, K. T. Tan, Y. Gong, Y. Chen, Z. Li, S. Xie, T. He, Z. Lu, H. Yang and D. Jiang, *Chem. Soc. Rev.*, 2021, **50**, 120–242.
- 5 S. Kandambeth, K. Dey and R. Banerjee, *J. Am. Chem. Soc.*, 2019, **141**, 1807–1822.
- 6 (a) E. Jin, M. Asada, Q. Xu, S. Dalapati, M. A. Addicoat, M. A. Brady, H. Xu, T. Nakamura, T. Heine, Q. Chen and D. Jiang, *Science*, 2017, **357**, 673–676; (b) E. Jin, J. Li, K. Geng, Q. Jiang, H. Xu, Q. Xu and D. Jiang, *Nat. Commun.*, 2018, **9**, 4143; (c) S. Bi, C. Yang, W. Zhang, J. Xu, L. Liu, D. Wu, X. Wang, Y. Han, Q. Liang and F. Zhang, *Nat. Commun.*, 2019, **10**, 2467.
- 7 P.-L. Wang, S.-Y. Ding, Z.-C. Zhang, Z.-P. Wang and W. Wang, *J. Am. Chem. Soc.*, 2019, **141**, 18004–18008.
- 8 X.-T. Li, J. Zou, T.-H. Wang, H.-C. Ma, G.-J. Chen and Y.-B. Dong, *J. Am. Chem. Soc.*, 2020, **142**, 6521–6526.
- 9 B.-J. Yao, W.-X. Wu, L.-G. Ding and Y.-B. Dong, *J. Org. Chem.*, 2021, **86**, 3024–3032.
- 10 (a) X. Kan, J.-C. Wang, Z. Chen, J.-Q. Du, J.-L. Kan, W.-Y. Li and Y.-B. Dong, *J. Am. Chem. Soc.*, 2022, **144**, 6681–6686; (b) J.-C. Wang, X. Kan, J.-Y. Shang, H. Qiao and Y.-B. Dong, *J. Am. Chem. Soc.*, 2020, **142**, 16915–16920.
- 11 J. Liu, T. Yang, Z.-P. Wang, P.-L. Wang, J. Feng, S.-Y. Ding and W. Wang, *J. Am. Chem. Soc.*, 2020, **142**, 20956–20961.
- 12 (a) X.-T. Li, J. Zou, Q. Yu, Y. Liu, J.-R. Li, M.-J. Li, H.-C. Ma, G.-J. Chen and Y.-B. Dong, *Chem. Commun.*, 2022, **58**, 2508–2511; (b) L.-G. Ding, S. Wang, B.-J. Yao, W.-X. Wu, J.-L. Kan, Y. Liu, J. Wu and Y.-B. Dong, *J. Mater. Chem. A*, 2022, **10**, 3346–3358.
- 13 W.-X. Wu, F. Li, B.-J. Yao, L.-G. Ding, J.-L. Kan, F. Liu, G.-Y. Zhao, S. Wang and Y.-B. Dong, *J. Hazard. Mater.*, 2022, **433**, 128831.
- 14 G.-B. Wang, Y.-J. Wang, J.-L. Kan, K.-H. Xie, H.-P. Xu, F. Zhao, M.-C. Wang, Y. Geng and Y.-B. Dong, *J. Am. Chem. Soc.*, 2023, **145**, 4951–4956.
- 15 (a) C. Mannich and W. Krösche, *Arch. Pharm.*, 1912, **250**, 647–667; (b) C. Mannich, *J. Chem. Soc. Abstr.*, 1917, **112**, 634; (c) M. Arend, B. Westermann and N. Risch, *Angew. Chem., Int. Ed.*, 1998, **37**, 1044–1070; (d) S. Shi, W. Qiu, P. Miao, R. Li, X. Lin and Z. Sun, *Nat. Commun.*, 2021, **12**, 1006; (e) C. Cheng, Y. Liu, G. Sheng, X. Jiang, X. Kang, C. Jiang, Y. Liu, Y. Zhu and Y. Cui, *Angew. Chem., Int. Ed.*, 2024, e202403473.
- 16 (a) G.-B. Wang, K.-H. Xie, H.-P. Xu, Y.-J. Wang, F. Zhao, Y. Geng and Y.-B. Dong, *Coord. Chem. Rev.*, 2022, **472**, 214774; (b) Y.-N. Gong, X. Guan and H.-L. Jiang, *Coord. Chem. Rev.*, 2023, **475**, 214889; (c) H. Zhao, Y. Wang,



- F. Zhang, X. Dong and X. Lang, *Appl. Catal., B*, 2024, **350**, 123899.
- 17 Materials Studio Release Notes; *Accelrys Software*, 2018.
- 18 A. Bhunia, I. Boldog, A. Möller and C. Janiak, *J. Mater. Chem. A*, 2013, **1**, 14990–14999.
- 19 G.-B. Wang, S. Li, C.-X. Yan, F.-C. Zhu, Q.-Q. Lin, K.-H. Xie, Y. Geng and Y.-B. Dong, *J. Mater. Chem. A*, 2020, **8**, 6957–6983.
- 20 (a) R. B. Wagh and J. M. Nagarkar, *Tetrahedron Lett.*, 2017, **58**, 3323–3326; (b) J. H. P. Tyman. *Synthetic and Natural Phenols*. New York: Elsevier, 1996; (c) L. Pilato, *React. Funct. Polym.*, 2013, **73**, 270–277; (d) Y. Ji, P. Li, X. Zhang and L. Wang, *Org. Biomol. Chem.*, 2013, **11**, 4095–4101.
- 21 (a) X. Yan, H. Liu, Y. Li, W. Chen, T. Zhang, Z. Zhao, G. Xing and L. Chen, *Macromolecules*, 2019, **52**, 7977–7983; (b) S. Sau and S. K. Samanta, *Chem. Commun.*, 2023, **59**, 635–638; (c) S. P. Pitre, C. D. McTiernan, H. Ismaili and J. C. Scaiano, *J. Am. Chem. Soc.*, 2013, **135**, 13286–13289.

